Catalysis Today 138 (2008) 239–243

Contents lists available at ScienceDirect

Catalysis Today

journal homepage: www.elsevier.com/locate/cattod

Preferential CO oxidation in H_2-rich gas mixtures over Au/doped ceria catalysts

Maela Manzoli [a,*], George Avgouropoulos [b], Tatyana Tabakova [c], Joan Papavasiliou [b], Theophilos Ioannides [b], Flora Boccuzzi [a]

[a] Department of Chemistry IFM and NIS Centre of Excellence, University of Torino, via P. Giuria 7, 10125 Torino, Italy
[b] Foundation for Research and Technology-Hellas (FORTH), Institute of Chemical Engineering and High Temperature Chemical Processes (ICE-HT), P.O. Box 1414, GR-26504 Patras, Greece
[c] Institute of Catalysis, Bulgarian Academy of Sciences, Acad. G. Bonchev Str., bl. 11, 1113 Sofia, Bulgaria

ARTICLE INFO

Article history:
Available online 24 June 2008

Keywords:
Gold catalysts
Doped ceria
Preferential CO oxidation
FTIR
Raman

ABSTRACT

Nanosized gold catalysts supported on doped ceria were prepared by deposition–precipitation method. A deep characterization study by HRTEM/EDS, XRD, FT-Raman, TPR and FTIR was undergone in order to investigate the effect of ceria modification by various cations (Sm^{3+}, La^{3+} and Zn^{2+}) on structural and redox properties of gold catalysts. Doping of ceria affected in different way catalytic activity towards purification of H_2 via preferential CO oxidation. The following activity order was observed: Au/Zn–CeO_2 > Au/Sm–CeO_2 > Au/CeO_2 > Au/La–CeO_2. The differences in CO oxidation rates were ascribed to different concentration of metallic gold particles on the surface of Au catalysts (as confirmed by the intensity of the band at 2103 cm^{-1} in the FTIR spectra collected during CO–O_2 interaction). Gold catalysts on modified ceria showed improved tolerance towards the presence of CO_2 and H_2O in the PROX feed. The spectroscopic experiments evidence enhanced reactivity when PROX is performed in the presence of H_2O already at 90 K.

1. Introduction

The preferential CO oxidation (PROX) reaction in H_2-rich gas mixtures is a suitable route for the production of CO-free hydrogen for fuel cell systems. High reaction rate, high selectivity with respect to the undesired side reactions and stability towards deactivation are the most important requirements from a catalyst for the PROX reaction. Highly dispersed Au nanoparticles supported on selected metal oxides [1–3], were found to be superior than conventional Pt group or Cu-based catalysts, since they are able to remove CO from reformed fuels with an extraordinarily high reaction rate and good selectivity at much lower temperatures. CeO_2 is an attractive oxide with unique catalytic properties due its distinct defect chemistry and the ability to exchange lattice oxygen with the gas phase [4]. These properties include the promotion of the precious metal dispersion, the enhancement of the catalytic activity at the interfacial metal-support sites and the promotion of CO removal through oxidation employing lattice oxygen. Various additives, such as samaria, lanthana or zirconia have been incorporated in ceria lattice in order to improve its reducibility, oxygen mobility and thermal stability [4,5]. Earlier reports have shown that Au/ceria catalysts are very promising for PROX reactions [3,6–12]. These catalysts have exhibited high activity and good selectivity and stability at low temperatures. In a comparative study of ceria supported gold and copper catalysts some of us have reported that nanosized Au/CeO_2 is active for preferential CO oxidation, but the presence of CO_2 and H_2O decreases the catalytic activity [13].

In this work we have modified ceria by addition of various cations (Sm^{3+}, La^{3+} and Zn^{2+}) in order to obtain a defective fluorite structure with increased oxygen mobility that could result in activity enhancement and improved resistance towards deactivation caused by the presence of CO_2 and H_2O in the PROX feed. A detailed characterization study has been undertaken in order to investigate the effect of modification of ceria on structural properties of the catalysts and to find correlation with catalytic performance in the PROX reaction.

2. Experimental

Doped ceria supports were synthesized by a co-precipitation method in an automated reactor under complete control of all

* Corresponding author. Tel.: +39 0116707541; fax: +39 0116707855.
E-mail address: maela.manzoli@unito.it (M. Manzoli).

0920-5861/$ – see front matter © 2008 Elsevier B.V. All rights reserved.
doi:10.1016/j.cattod.2008.05.001

reaction parameters. Mixed aqueous solution of nitrate salts of cerium and metal modifier in atomic ratio M/(M + Ce) = 0.05 (M: Sm, Zn or La) and precipitating agent K_2CO_3 were added drop-wise in the reactor by maintaining a constant pH 9.0, temperature = 333 K. The precipitates were aged for 1 h at 333 K, filtered, washed carefully until absence of NO_3^- ions, dried under vacuum at 353 K and calcined in air at 673 K for 2 h. Gold catalysts were prepared by deposition–precipitation. Deposition of $Au(OH)_3$ onto the supports suspended ultrasonically in H_2O was carried out via interaction between $HAuCl_4{\cdot}3H_2O$ (Merck) and K_2CO_3 under vigorous stirring at constant pH 7.0 and at 333 K. After aging for 1 h, the precipitates were washed, dried in vacuum at 353 K and calcined in air at 673 K for 2 h. The actual gold loading for each catalyst was 3 ± 0.05 wt.%, as measured by atomic absorption analysis.

Fourier transform Raman (FT-Raman) measurements were obtained using a Bruker (D) FRA-106/S component attached to an EQUINOX 55 spectrometer. A R510 diode pumped Nd:YAG polarized laser at 1064 nm (with a maximum output power of 500 mW) was used for Raman excitation in a 180° scattering sample illumination module. An optical filtering reduced the Rayleigh elastic scattering and in combination with a CaF_2 beamsplitter and a high sensitivity liquid N_2 cooled Ge-detector allowed the Raman intensities to be recorded from 50 to 3000 cm^{-1} in Stokes-shifted Raman region, all in one spectrum. Spectra shown here are an average of 500 scans at 4 cm^{-1} resolution, while the intensity of the Nd:YAG on the sample was 250 mW.

The specific surface areas of the catalysts, S_{BET}, were determined from the adsorption isotherm of nitrogen at 77 K using a Quantachrome Autosorb-1 instrument.

Temperature-programmed reduction (TPR) experiments were performed in a typical flow system [14], equipped with a mass spectrometer (Omnistar/Pfeiffer Vacuum), under a flow of a 3% H_2/He mixture (50 cm^3 min^{-1}) over 50 mg of catalyst using a heating rate of 10 K min^{-1}.

The crystalline structure of the doped oxides was analyzed by means of an X-ray powder diffractometer (Bruker D8 Advance) employing Cu Kα radiation (λ = 0.15418 nm).

High-resolution electron transmission microscopy (HRTEM) analysis was performed using a JEOL 2000 EX electron microscope, equipped with a top entry stage and a LaB_6 filament. The powdered samples were ultrasonically dispersed in isopropyl alcohol and the obtained suspensions were deposited on a copper grid, coated with a porous carbon film.

Activity and selectivity measurements for the PROX process were carried out at atmospheric pressure, in the temperature range of 300–380 K, in a conventional fixed-bed reactor system [14]. The catalyst was in the form of powder with particle size in the range of $90 < dp < 180$ μm and mass of 120 mg and the total flow rate of the reaction mixture was 50 cm^3 min^{-1}, yielding $W/F = 0.144$ g s cm^{-3}. CO oxidation rates were measured in separate runs performed under differential conditions, with CO conversion <10–15% and catalyst mass of 10 mg diluted at a 5:1 ratio with inert sea sand. The feed always contained 1% CO, 1.25% O_2, 50% H_2 and He as balance. The effect of CO_2 and H_2O was examined with the addition of 15% CO_2 or/and 10% H_2O in the feed. Prior to all catalytic measurements, the samples were treated in a flowing: (a) 20 vol.% O_2/He mixture at 673 K for 30 min or (b) 10 vol.% H_2/He mixture at 373 K for 1 h, followed by cooling down to the reaction temperature in pure He. Product and reactant analysis was carried out by a gas chromatograph (Shimadzu GC-14B) equipped with a TCD. The CO conversion calculation was based on the CO_2 formation or CO consumption (when an excess of CO_2 was added). The selectivity towards CO_2 production was calculated from the oxygen mass balance.

The Fourier transformed infrared (FTIR) spectra were collected on a PerkinElmer 1760 spectrometer (equipped with a MCT detector) with the samples in self-supporting pellets introduced in a cell allowing thermal treatment in controlled atmospheres and spectrum scanning at controlled temperatures (from 90 K up to room temperature).

3. Results and discussion

3.1. Characterization of the doped and undoped supports

Fig. 1 shows the Raman spectra for Sm^{3+}-, La^{3+}- and Zn^{2+}-doped ceria supports and for pure CeO_2. An intense peak, that is characteristic of fluorite-type oxide structure of CeO_2 [15–19] is observed at 462 cm^{-1}. This peak shifted from 462 cm^{-1} (fine curve) to 454 cm^{-1} upon addition of dopants (bold, dashed and dotted curves). Doping by La mostly affected the fluorite structure of ceria, probably due to its highest ionic radius [20]. The main line of doped ceria becomes broader and weaker than that of pure CeO_2, a fact that may be related to a change of CeO_2 environment in the presence of dopants due to the formation of solid solutions [15–19]. The full width at half maximum (FWHM) of the main line of ceria in the Raman spectra increases from 31 cm^{-1} for pure CeO_2 to 35 cm^{-1} for Zn–CeO_2, 37 cm^{-1} for Sm–CeO_2 and 38 cm^{-1} for La–CeO_2. The change in Raman line width is indicative of an increase in the ceria dispersion or of larger amount of oxygen vacancies formed in ceria by the addition of dopant cations. An additional band is detected at about 580–590 cm^{-1} (see inset in Fig. 1). This feature has been attributed to the presence of defects (vacancies or impurities) in the structure and its area may be related to the oxygen vacancy concentration [15,17].

3.2. Textural properties of the catalysts

N_2 physisorption results showed that pure ceria has a specific surface area of 70 m^2 g^{-1}, which decreases to 65 m^2 g^{-1} after gold deposition. However, a decrease of S_{BET} is observed when ceria is modified with Zn^{2+} (63 m^2 g^{-1}), Sm^{3+} (54 m^2 g^{-1}) and La^{3+} (53 m^2 g^{-1}). Particularly, the largest impact was detected after doping with 3+ ions of La and Sm. Moreover, XRD analysis evidenced that a fraction of Sm^{3+}, La^{3+} and Zn^{2+} cations gets incorporated into the CeO_2 lattice, leading to solid solution formation (data not shown for the sake of brevity). The calculation of the main crystallite sizes of CeO_2 from line broadening of CeO_2 (1 1 1) using Scherrer's equation indicated that all additives inhibit

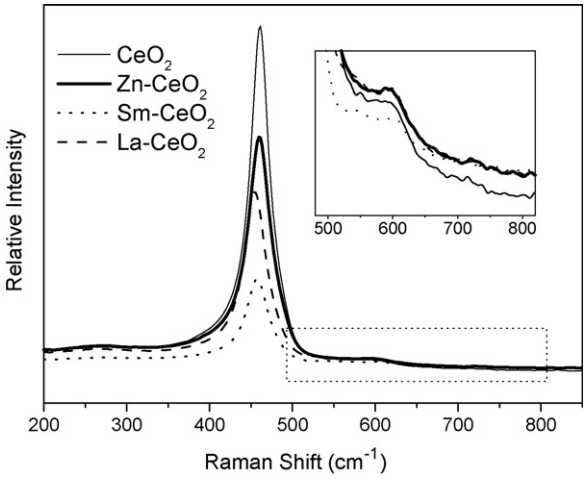

Fig. 1. Raman spectra of the samples excited by 1064 nm laser line.

the crystal growth of ceria and favor the production of smaller particles. The calculated values (CeO_2: 7 nm, Au/CeO_2: 6.2 nm, Au/La–CeO_2: 5 nm, Au/Sm–CeO_2: 5 nm, and Au/Zn–CeO_2: 5.1 nm) corroborated Raman spectroscopy data for increase of ceria dispersion after doping. Taking into account the XRD patterns of the doped catalysts and in agreement with previous studies of some of us [20,21], it can be said that with the incorporation of a cation with higher ionic radius than that of Ce^{4+}, such as La^{3+} or Sm^{3+}, the XRD reflections of the doped ceria are shifted to lower degrees. On the other hand, the reflections are shifted to higher degrees with the incorporation of a cation with smaller ionic radius than that of Ce^{4+}, e.g. Zn^{2+}.

HRTEM analysis revealed big Au agglomerates with size of at least 10 nm and very highly dispersed clusters with size of about 1 nm on Au/CeO_2, whose presence was confirmed by EDS. On the contrary, only gold particles with size around 3.5–4 nm have been found on Au/Sm–CeO_2 and with size of about 5 nm on Au/La–CeO_2. However, a particle size distribution cannot be provided due to the very hard detection of gold on nanocrystalline ceria. Finally, no Au particles have been observed on Au/Zn–CeO_2. Taking into account that all samples have the same metal loading (3 wt.%), this feature may indicate that Au dispersion on this catalyst is higher than that on Au/Sm–CeO_2.

As for TPR measurements, a single peak centered at ~396 K was observed for Au/ceria, while the TPR peak of the doped catalysts is shifted either to lower (Au/Sm–CeO_2 and Au/Zn–CeO_2, 377 and 380 K, respectively) or to higher temperatures (Au/La–CeO_2, 408 K).

3.3. Catalytic activity and selectivity in the PROX reaction

The comparison of the activity and the selectivity in the PROX reaction for all catalysts after oxidative and reductive pretreatment is reported in Table 1. These data were also collected in the presence of either CO_2 or CO_2 and H_2O in the PROX mixture. In addition, the CO oxidation rates, r_{CO}, were measured under differential conditions, with CO conversion lower than 10–15%. The corresponding results pertaining to the mixture containing water are not reported in Table 1 since it was very difficult to obtain differential rates in the presence of H_2O because of the large error in the quantification of small changes in the CO or CO_2 concentration (in order to avoid condensation problems, those rates should be obtained at much higher temperatures, where H_2 oxidation dominates). The results reported in Table 1 clearly indicate that addition of a dopant in the catalyst composition affected in a different way the catalytic performance. Particularly, Sm- and Zn-doped Au/ceria showed almost the same PROX activity and are more active than undoped Au/ceria. On the contrary, the insertion of La did not improve the catalyst's performance. However, a reductive pretreatment at 373 K for 1 h has a positive effect on the activity. Finally, the presence of dopants improved the tolerance of the catalysts towards 15% CO_2 in the reaction mixture, even if the catalytic activity is decreased, and the co-presence of 10% H_2O in the same mixture enhanced the catalytic activity of all catalysts. It could be suggested that water is able to compensate completely the negative effect caused by CO_2, as evidenced by IR spectroscopic data collected in the presence of water in PROX mixture, reported below.

3.4. Interaction of the reduced catalysts with CO, oxygen and the PROX mixture at 90 K

The abundance of defect sites at the surface of the reduced doped and undoped catalysts was monitored by FTIR spectroscopy. The FTIR absorbance spectra of Au/CeO_2 (fine curve), Au/Zn–CeO_2 (bold curve) and Au/La–CeO_2 (dashed curve) undergone to a reduction in H_2 at 373 K are shown in Fig. 2a. We do not report the spectrum related to Au/Sm–CeO_2 since it is a duplicate of that of Au/Zn–CeO_2. All spectra have been normalized to the weight of the pellets. The aim was to compare the band at 2129 cm^{-1} related to the forbidden $^2F_{5/2} \rightarrow {}^2F_{7/2}$ electronic transition of Ce^{3+}[22] in order to have information on the abundance of the defect sites at the catalysts surface. The intensity follows the order: Au/CeO_2 > Au/Zn–CeO_2 (≈Au/Sm–CeO_2) > Au/La–CeO_2. Moreover, the FTIR absorbance spectra, normalized to the weight of the pellets, of the same samples are reported in Fig. 2c, after O_2 adsorption at 90 K. A band at 1135 cm^{-1} is observed on all catalysts. This band has been assigned to the stretching mode of a superoxo-species O_2^- [23]. Also in this case, the strongest intensity is detected on the undoped sample (fine curve), while the weakest intensity is measured on the La-doped sample (dashed curve) and an intermediate intensity is observed as for the Zn (and Sm)-doped one (bold curve), indicating that their amount is strictly connected to that of Ce^{3+} surface-defective sites.

The FTIR spectra collected after CO adsorption at 90 K on the catalysts previously reduced in H_2 at 373 K are compared in Fig. 2b. CO adsorption on the reduced samples is of particular interest, because PROX activity tests have shown that a reductive pretreatment promotes the catalytic activity. The bands observed in the range 2170–2140 cm^{-1} are related to Ce^{4+} and Ce^{3+} cations and to CO in interaction with the OH groups of the support. At lower frequencies, the admission of CO at 90 K on the La-containing catalyst produced a band centred at 2100 cm^{-1}, assigned to CO on Au^0 sites. On the Sm- and Zn-doped catalysts this absorption is red shifted with respect to the usual position of metallic gold at 2100 cm^{-1}, at about 2095 cm^{-1} and showed a component at lower

Table 1
Comparison of the catalysts performance in the PROX reaction

Catalyst	Treatment	1% CO, 1.25% O_2, 50% H_2, He			+15% CO_2			Maximum activity[a] (%)
		r_{CO} at 323 K ($\mu mol\ s^{-1}\ g_{cat}^{-1}$)	E_a (kJ mol^{-1})	Maximum activity[a] (%)	r_{CO} at 323 K ($\mu mol\ s^{-1}\ g_{cat}^{-1}$)	E_a (kJ mol^{-1})	Maximum activity[a] (%)	+15% CO_2, 10% H_2O
Au/CeO_2	Oxidation	9.4	38.3		1.5	47.0		
	Reduction	11.8	36.2	96.6 (58) at 323 K	1.9	43.2	70 (31) at 353 K	78 (59) at 348 K
Au/Zn–CeO_2	Oxidation	13.5	31.3					
	Reduction	15.1	29.1	100 (47) at 323 K	4.8	33.9	94.5 (50) at 323 K	99.9 (55) at 338 K
Au/Sm–CeO_2	Oxidation	12.3	33.0					
	Reduction	13.9	31.4	99 (44) at 323 K	4.3	35.8	93.4 (41) at 323 K	96.6 (46) at 338 K
Au/La–CeO_2	Oxidation	7.3	40.5					
	Reduction	8.8	37.5	95.4 (42) at 338 K	2.5	41.4	84.6 (47.8) at 343 K	93.1 (55) at 353 K

[a] Activity expressed as CO conversion at W/F = 0.144 g s cm^{-3}. The values in parenthesis denote the % selectivity towards CO_2 production.

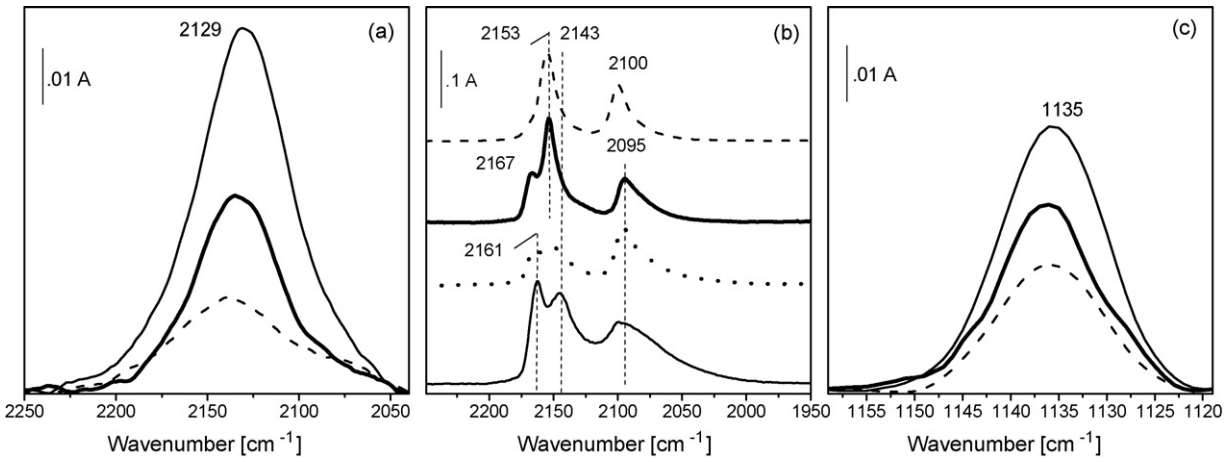

Fig. 2. FTIR absorbance spectra of Au/CeO_2 (fine curve), $Au/Zn–CeO_2$ (bold curve) and $Au/La–CeO_2$ (dashed curve) undergone to a reduction in H_2 at 373 K (a) and after O_2 interaction at 90 K (c). (b) Comparison of the FTIR difference spectra of the samples reduced in H_2 at 373 K and in contact with 0.5 mbar CO at 90 K: Au/CeO_2 (fine curve), $Au/Zn–CeO_2$ (bold curve), $Au/Sm–CeO_2$ (dotted curve) and $Au/La–CeO_2$ (dashed curve). The spectra have been normalized either to the weight of the pellets (a and c) or the Au content (b).

frequencies. These bands can be related to CO adsorbed on small Au particles and clusters, respectively. Moreover, these species are negatively charged, due to an electronic transfer from the reduced supports to the metal [24,25]. The absorption becomes larger and more complex on the undoped catalyst. All spectroscopic features may be correlated with HRTEM data that reveal prevailing presence of gold clusters on the surface of Au/CeO_2 and mainly particles with different size on the modified Au/CeO_2 catalysts.

FTIR spectra were collected during $CO–O_2$ interaction in order to explore the effect of ceria modification on the activity of the catalysts. Oxygen was admitted on CO preadsorbed at 90 K on the reduced catalysts. Significant changes are observed after 20 min (Fig. 3). The production of CO_2 is evidenced by the strong band at 2340 cm^{-1}. It can be seen that this band is most intense in the spectra of $Au/Zn–CeO_2$ and $Au/Sm–CeO_2$. This observation is of particular importance, because it correlates well with the registered higher CO oxidation rate of above-mentioned two catalysts. The presence of metallic gold particles on the surface of these modified Au catalysts (as confirmed by the higher intensity of the band at 2103 cm^{-1}) reveals the decisive role of metallic gold in CO oxidation reactions. At the same time the lowest intensity of the band, related to CO adsorption on metallic gold particles on the surface of $Au/La–CeO_2$ agrees with the lowest catalytic performance of this sample. In low-frequency range, the band at 1135 cm^{-1}, assigned previously to a superoxo-species O_2^- [23], is observed on all catalysts.

We also studied by FTIR the PROX reaction at 90 K on $Au/Zn–CeO_2$, which is the most active, as indicated by the catalytic tests. Firstly, an excess of H_2 was contacted with the sample. Then the cell was cooled at 90 K and a mixture of CO and O_2 (1:1) was introduced at the same temperature. The evolution within 20 min has been followed by FTIR (spectra not shown). In Fig. 4 the spectra collected after 20 min of interaction between either the PROX mixture (bold curve) or the same mixture in the presence of H_2O (fine curve) with $Au/Zn–CeO_2$ are reported. For the sake of clarity, both spectra have been normalised with respect to the weight of the pellets. A broad adsorption band appeared in the high frequency range (not shown) due to the OH stretching modes when H_2O was added to the mixture. As evidenced by the band at 2340 cm^{-1}, CO_2 is produced already at 90 K in both cases and the

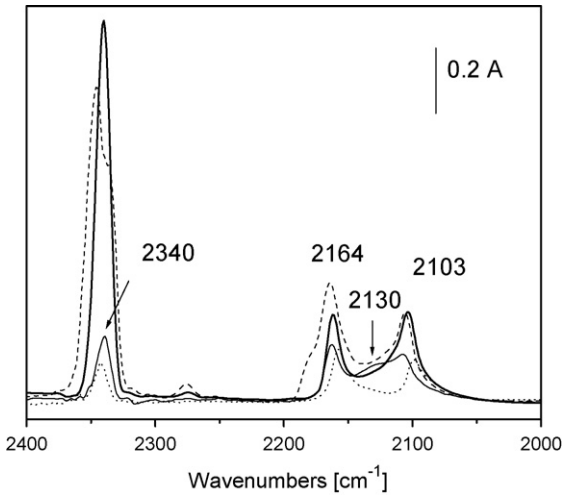

Fig. 3. FTIR adsorption spectra after admission of O_2 at 90 K on 0.5 mbar CO preadsorbed on the reduced catalysts: Au/CeO_2 (fine curve), $Au/Zn–CeO_2$ (bold curve), $Au/Sm–CeO_2$ (dashed curve) and $Au/La–CeO_2$ (dotted curve) after 20 min of interaction. All spectra are normalized to the weight of the pellet.

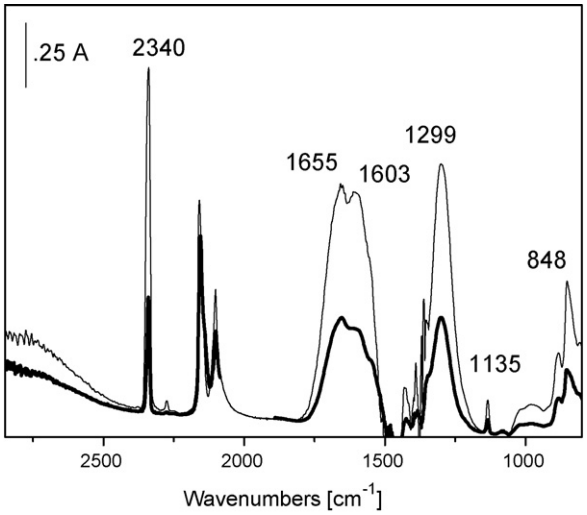

Fig. 4. Comparison between the FTIR spectra recorded after 20 min of interaction at 90 K on $Au/Zn–CeO_2$ in $CO–O_2–H_2$ (1:1:7) mixture (bold curve) and after addition of water to $CO–O_2–H_2$ (1:1:7) mixture (fine curve). The spectra are normalized to the weight of the pellets.

band is more intense in the presence of water. Moreover, the nature and the relative intensities of the absorption bands in the carbonylic stretching region, extending in the range 2250–2000 cm^{-1}, are similar to those observed in the absence of water (fine and bold curve, respectively). Bands, related to carbonate species, are formed in the 1800–800 cm^{-1} region. These species are more abundant when water is added (fine curve). Moreover, the band at 1135 cm^{-1}, related to O_2^- species [23] was observed after interaction with both mixtures. The presence of these species can be taken as an indication for the ability of the catalysts to activate O_2 already at low temperature. A pronounced effect of water on the CO oxidation rate in PROX reaction even at room temperature has been found for $Au/MO_x/Al_2O_3$ (M = Mg, Mn) [26]. Schubert et al. have studied the effects of CO_2 and H_2O on PROX over Au/α-Fe_2O_3 and reported reduction of CO oxidation rate after addition of CO_2, while in the presence of water the reaction rate is accelerated [2].

3.5. Characterization results and PROX catalytic activity: concluding remarks

The addition of Zn^{2+}, Sm^{3+} and La^{3+} dopants to the Au/CeO_2 composition influenced differently the catalytic activity in the PROX reaction. More specifically, they caused either an increase (Sm- and Zn-doped catalysts) or a decrease (La-doped catalysts) of activity. Moreover, doping of ceria had a beneficial effect on CO_2 and H_2O tolerance of doped gold catalysts. The origin of the observed differences can be related to a modification of the defective structure of ceria. The Raman data collected along the characterization of the bare supports allowed to evidence a change of CeO_2 environment in the presence of dopants due to the formation of solid solutions as well as increase of the number of oxygen vacancies formed in the lattice of ceria [15,17,19]. FTIR spectroscopic findings indicate that the concentration of Ce^{3+}-defective sites is higher on the surface of Au/CeO_2 than on Au/Sm- and Zn-doped ceria. The trend is opposite than that concerning experimental catalytic results for CO oxidation rate, where an enhancement by Au/Sm- and Zn-doped ceria catalysts is observed. Indeed, FTIR spectra showed the largest intensity and broadness of the absorption related to CO on gold for reduced Au/CeO_2, indicating the presence of Au clusters on the surface of this catalyst. This result may imply that gold clusters and Ce^{3+}-defective sites are not the active sites in the PROX reaction, while the step sites of gold particles are the active sites for both CO and oxygen activation and play a decisive role in the PROX reaction. TPR measurements on the doped and undoped catalysts evidenced a different reducibility of the materials, also indirectly confirmed by the different relative intensities of the FTIR CO bands related to Ce^{4+} and Ce^{3+} on the catalysts after reduction and depending possibly from differences in the gold dispersion, as shown by the HRTEM analysis. One of the most often debated question concerns identification of active sites in CO oxidation reaction—whether ionic or metallic gold is the active species. FTIR spectra, collected during $CO–O_2$ interaction at 90 K evidence the important role of metallic gold particles. The following order of intensity of the band at 2103 cm^{-1}, ascribed to CO adsorption on metallic gold particles was observed: $Au/Zn–CeO_2 \approx Au/Sm–CeO_2 > Au/CeO_2 > Au/La–CeO_2$. Moreover, larger amounts of CO_2 during CO oxidation were produced in the presence of gold particles on the surface of Zn- and Sm-modified Au catalysts. The catalytic performance in PROX demonstrated the same activity trend and demonstrates the key role of metallic gold for the achievement of high CO oxidation rates. As for the reactivity, the spectroscopic experiments showed that when PROX is performed in the presence of H_2O, more molecular CO_2 and carbonate species are produced, indicating that the reactivity is enhanced by the presence of water already at 90 K. Neither formates nor bicarbonates, indicative of reactions of H_2, are produced during PROX and PROX in the presence of water.

Acknowledgements

M.M. and F.B. gratefully acknowledge the COFIN 2006. J.P., G.A. and T.I. are grateful to the Ministry of Development, General Secretariat for Research and Technology-Greece for the financial support in the frame of the Greece-Bulgaria bilateral S&T cooperation program. T.T. gratefully acknowledges the financial support of the Ministry of Education and Science, National Science Fund-Bulgaria (Project BG-7). The authors from FORTH/ICE-HT would also like to thank Dr. A. Soto for assisting with the Raman experiments.

References

[1] G. Avgouropoulos, T. Ioannides, Ch. Papadopoulou, J. Batista, S. Hocevar, H. Matralis, Catal. Today 75 (2002) 157.
[2] M.M. Schubert, A. Venugopal, M.J. Kahlich, V. Plzak, R.J. Behm, J. Catal. 222 (2004) 32.
[3] W. Deng, J. De Jesus, H. Saltsburg, M. Flytzani-Stephanopoulos, Appl. Catal. A: Gen. 291 (2005) 126.
[4] A. Trovarelli, Catal. Rev.-Sci. Eng. 38 (1996) 439.
[5] M. Mogensen, N.M. Sammes, G.A. Tompsett, Solid State Ionics 129 (2000) 63.
[6] L. Chang, N. Sasirekha, Y. Chen, W. Wang, Ind. Eng. Chem. Res. 45 (2006) 4927.
[7] G. Panzera, V. Modafferi, S. Candamano, A. Donato, F. Frusteri, P.L. Antonucci, J. Power Sources 135 (2004) 177.
[8] A. Luengnaruemitchai, S. Osuwan, E. Gulari, Int. J. Hydrogen Energy 29 (2004) 429.
[9] O. Goerke, P. Pfeifer, K. Schubert, Appl. Catal. A: Gen. 263 (2004) 11.
[10] A. Jain, X. Zhao, S. Kjergaard, S.M. Stagg-Williams, Catal. Lett. 104 (2005) 191.
[11] F. Arena, P. Famulari, G. Trunfio, G. Bonura, F. Frusteri, L. Spadaro, Appl. Catal. B: Environ. 66 (2006) 81.
[12] E. Ko, E.D. Park, K.W. Seo, H.C. Lee, D. Lee, S. Kim, Catal. Today 116 (2006) 377.
[13] G. Avgouropoulos, J. Papavasiliou, T. Tabakova, V. Idakiev, T. Ioannides, Chem. Eng. J. 124 (2006) 41.
[14] G. Avgouropoulos, T. Ioannides, Appl. Catal. A: Gen. 244 (2003) 155.
[15] J.E. Spanier, R.D. Robinson, F. Zhang, S.-W. Chan, I.P. Herman, Phys. Rev. B 64 (2001) 245407.
[16] G.W. Graham, W.H. Weber, C.R. Peters, R. Usmen, J. Catal. 130 (1991) 310.
[17] G. Marban, A.B. Fuertes, Appl. Catal. B: Environ. 57 (2004) 43.
[18] W. Shan, Z. Feng, Z. Li, J. Zhang, W. Shen, C. Li, J. Catal. 228 (2004) 206.
[19] D. Andreeva, P. Petrova, J.W. Sobczak, L. Ilieva, M. Abrashev, Appl. Catal. B: Environ. 67 (2006) 237.
[20] J. Papavasiliou, G. Avgouropoulos, T. Ioannides, Appl. Catal. B: Environ. 69 (2007) 226.
[21] T. Tabakova, V. Idakiev, J. Papavasiliou, G. Avgouropoulos, T. Ioannides, Catal. Commun. 8 (2007) 101.
[22] C. Binet, M. Daturi, J.C. Lavalley, Catal. Today 50 (1999) 207.
[23] V.V. Pushkarev, V.I. Kovalchuk, J.L. d'Itri, J. Phys. Chem. B 108 (2004) 5341.
[24] T. Tabakova, F. Boccuzzi, M. Manzoli, D. Andreeva, Appl. Catal. A: Gen. 252 (2003) 385.
[25] T. Tabakova, F. Boccuzzi, M. Manzoli, J.W. Sobczak, V. Idakiev, D. Andreeva, Appl. Catal. B: Environ. 49 (2004) 73.
[26] R.J.H. Grisel, B.E. Nieuwenhuys, J. Catal. 199 (2001) 48.